Supporting Information:

Facile Synthesis of Porous Transition Metal Hydroxides from Poly(4-vinyl pyridine) Film by Controlling pH

Gyeongwon Ha‡[1], Jaeyong Lee‡[1], Keon-Woo Kim[1], Chungryong Choi[2] and Jin Kon Kim*[1]

[1]National Creative Research Initiative Center for Hybrid Nano Materials by High-level Architectural Design of Block Copolymer, Department of Chemical Engineering, Pohang University of Science and Technology, Pohang, Republic of Korea

[2] Department of Polymer Science and Engineering, Kumoh National Institute of Technology, 61 Daehak-ro, Gumi, Gyeongbuk39177, Republic of Korea.

‡GH, JL are contributed equally.

*Correspondence and requests for materials should be addressed to J.K.K. (e-mail: jkkim@postech.ac.kr)

S1. Synthesis of P4VP

Synthetic routes of P4VP *via* RAFT polymerization are shown in scheme S1.

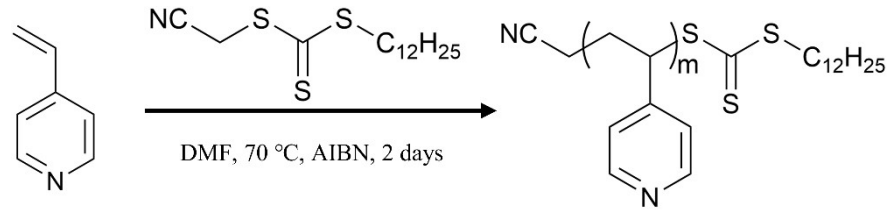

Scheme S1. Synthetic routes for P4VP by RAFT polymerization

10.48 mL (9.72 x 10^{-2} mol) of 4-vinyl pyridine, 50 mg (1.2 x 10^{-4} mol) of the RAFT agent cyanomethyl dodecyl trithiocarbonate (CMDTTC), and 5 mg (3 x 10^{-5} mol) of AIBN were added to a dry and argon-purged polymerization tube. For 30 min, the homogeneous solution was degassed under argon. A preheated warmed oil bath at 70 °C was used for polymerization tube for 48 h and the reaction was quenched by freezing the polymerization tube in liquid nitrogen. We used a very small amount of the reactant mixture to measure the monomer conversion using ^{1}H-NMR. The remaining mixture was diluted in 3 mL DMF, precipitated from 400 mL diethyl ether, and then dried under vacuum for 24 h at room temperature. Monomer conversion was 58 % determined by ^{1}H-NMR.

^{1}H-NMR (400 MHz, $CDCl_3$) δ [ppm]: 1.10-1.50 (broad, P4VP polymer backbone), 3.0-.3.2 (broad, -CH_2CN end-group), 6.0-.6.5 (broad, aromatic group), 8.0-.8.4 (broad, -N=CH in aromatic group). (Figure S1a)

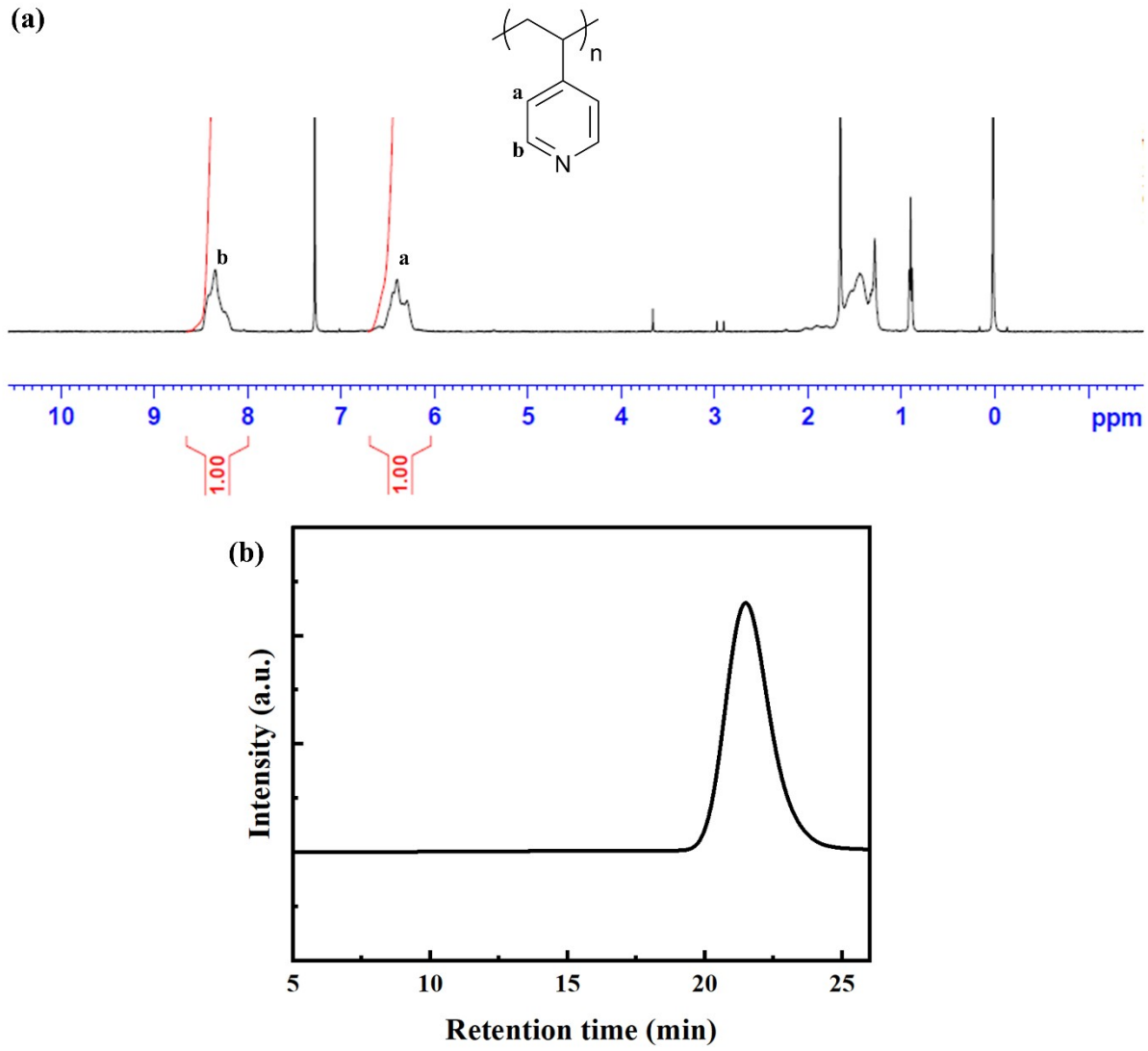

Figure S1. (a) ^{1}H-NMR spectra in $CDCl_3$ solvent and (b) SEC trace in DMF of synthesized P4VP.

S2. Thickness Change after Coordination.

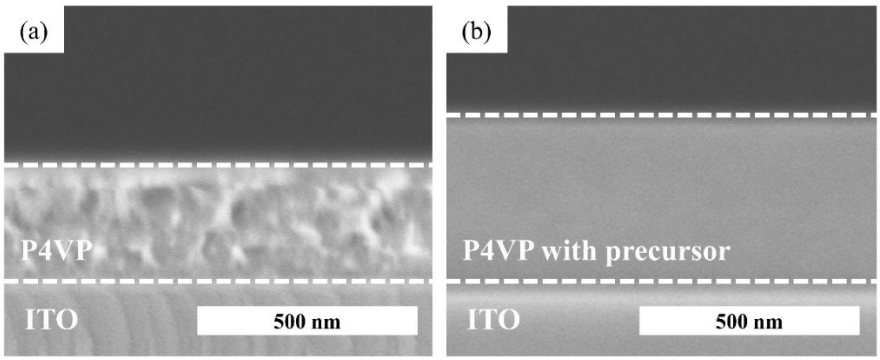

Figure S2. Cross-sectional views of FESEM images of P4VP film (a) before and (b) after dipping in $K_2Ni(CN)_4$ solution. The thickness of P4VP films before and after dipping followed by drying was 260 nm and 380 nm, respectively.

Since there was no void in the film after the coordination, we assume that the increased film thickness originated from the volume of coordinated precursors, as P4VP chains were stretching. We calculated the number of coordinated nitrogen atoms in the P4VP film. If the precursors were coordinated with all nitrogen in P4VP film, the number of nitrogen atom would be the same as the number of cyanide precursors.

$$\frac{A \times H_{P4VP} \times \rho_{P4VP}}{M_{4VP}} = \frac{A \times (H_{coordinated\ P4VP} - H_{P4VP}) \times \rho_{precursor}}{M_{precursor}} \quad \text{(S1)}$$

where A is the surface area of the film, H_i is the thickness of the film, ρ_i is the density of component *i, and* M_i is molar mass of component *i.* Here, we used density of P4VP of 1.15 g/cm^3 (ρ_{P4VP}) and cyanide precursor of 1.85 g/cm^3 ($\rho_{precursor}$). Also, the molar mass of 4VP was 104 g/mol and nickel cyanide precursor is 240 g/mol.

When H_{P4VP} is 260 nm (Figure S2a), $H_{coordinated\ P4VP} - H_{P4VP}$ would be 373 nm from Eq (S1) if the precursors were fully coordinated. However, since the final thickness was 380 nm (Figure S2b), $H_{coordinated\ P4VP} - H_{P4VP}$ should 120 nm, which implies 31 % of the number of nitrogen atoms in P4VP film was coordinated with the metal cyanide precursor. Therefore, 31 vol % of the coordinated film contained metal precursors and 69 vol % of the film consisted of uncoordinated P4VP homopolymer.

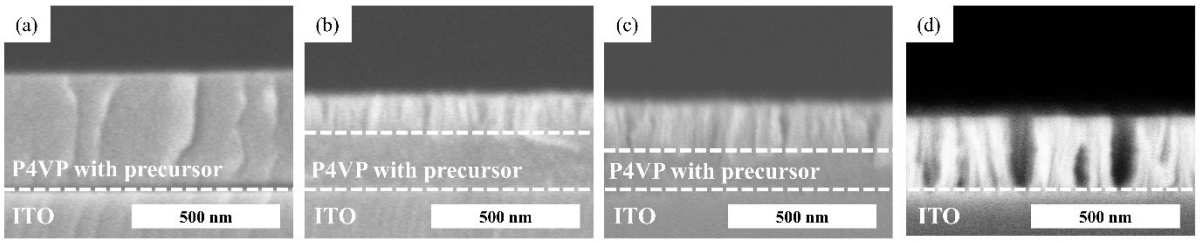

Figure S3. Cross-sectional views of FESEM images of porous nickel hydroxide film prepared from $K_2Ni(CN)_4$ solution with pH = 5 depending on O_2 RIE time: (a) before RIE, (b) 1 min, (c) 2 min, and (d) 5 min.

Figure S3 gives cross-sectional FESEM images of porous nickel hydroxide film depending on O_2 RIE time. With increasing RIE time, the total film thickness gradually decreased because of the etching of uncoordinated P4VP film. The total film thickness was 320 nm at 1

min RIE, 300 nm at 2 min RIE, and finally 240 nm at 5 min RIE, while original film thickness before RIE was 380 nm.

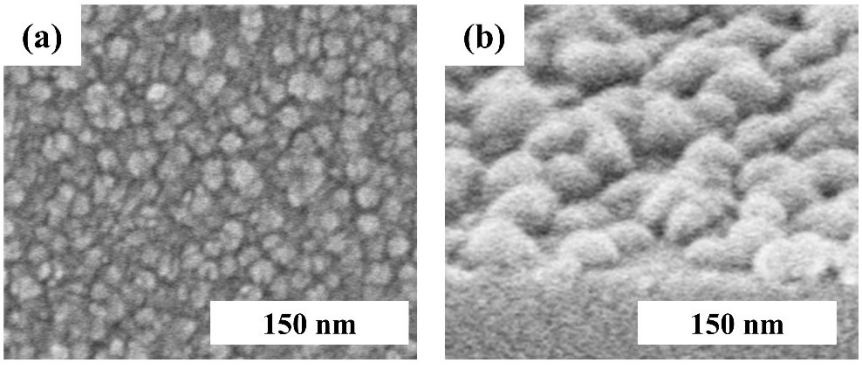

Figure S4. Top (a) and 60° tilt (b) views of FESEM image of structures prepared by heat treatment alone at 350℃ without O_2 RIE after dipping in $K_2Ni(CN)_4$ solution with pH = 5.

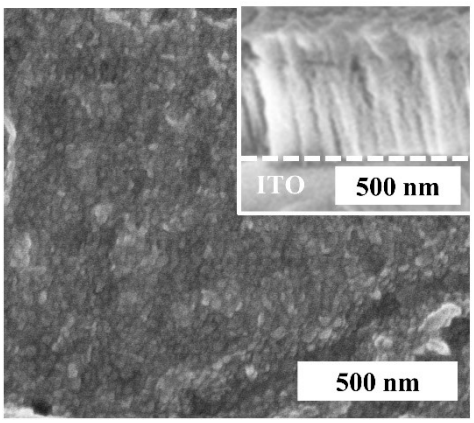

Figure S5. Top and 60° tilt (inset) views of FESEM image of $Ni(OH)_2$ structures prepared from $K_2Ni(CN)_4$ solution with pH = 4.

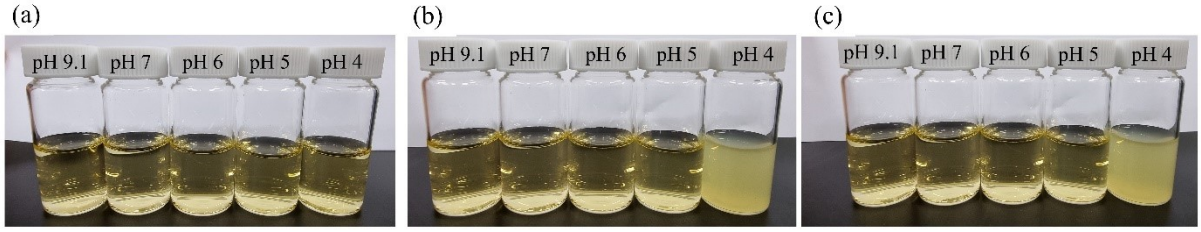

Figure S6. Changes in $K_2Ni(CN)_4$ solutions with various pH over time. (a) as dissolved, (b) after 1 min, (c) after 20 min.

Figure S6 shows changes in $K_2Ni(CN)_4$ solutions with various pH over time. For solutions with pH from 9.1 (DI water) to 5, all solutions appeared transparent even at long times. Thus, there is no precipitated nickel cyanide. However, for a precursor solution with pH = 4, a turbid solution was observed even at a very short time (1 min). This implies that a large amount of nickel cyanide was formed as the precipitate. Because this precipitate prevents effective coordination between N^+ and metal cyanide precursor, porous metal hydroxide structures were not formed, as shown in Figure S4.

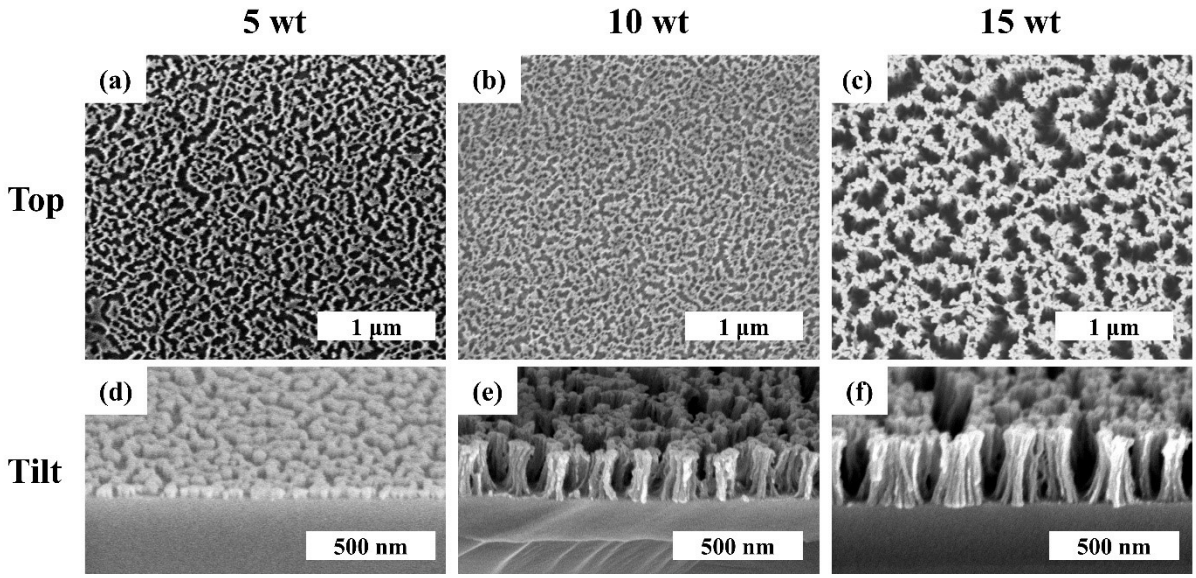

Figure S7. Top (upper panel) and 60° tilt (lower panel) views of FESEM images of $Ni(OH)_2$ structures as a function of initial P4VP film thickness prepared by spin-coating at 3000 rpm of different P4VP concentrations in DMF. (a, d) 5 wt%, (b, e) 10 wt%, (c, f) 15 wt%.

Figure S7 shows $Ni(OH)_2$ structures depending on the initial P4VP film thickness. The film thickness was controlled by the concentration P4VP in DMF. Porous $Ni(OH)_2$ structures were formed regardless of initial P4VP film thickness. Also, as expected, the height of porous $Ni(OH)_2$ structures increased with increasing initial P4VP film thickness. However, as the thickness increases, the structures are more likely to cluster together and form large pores.

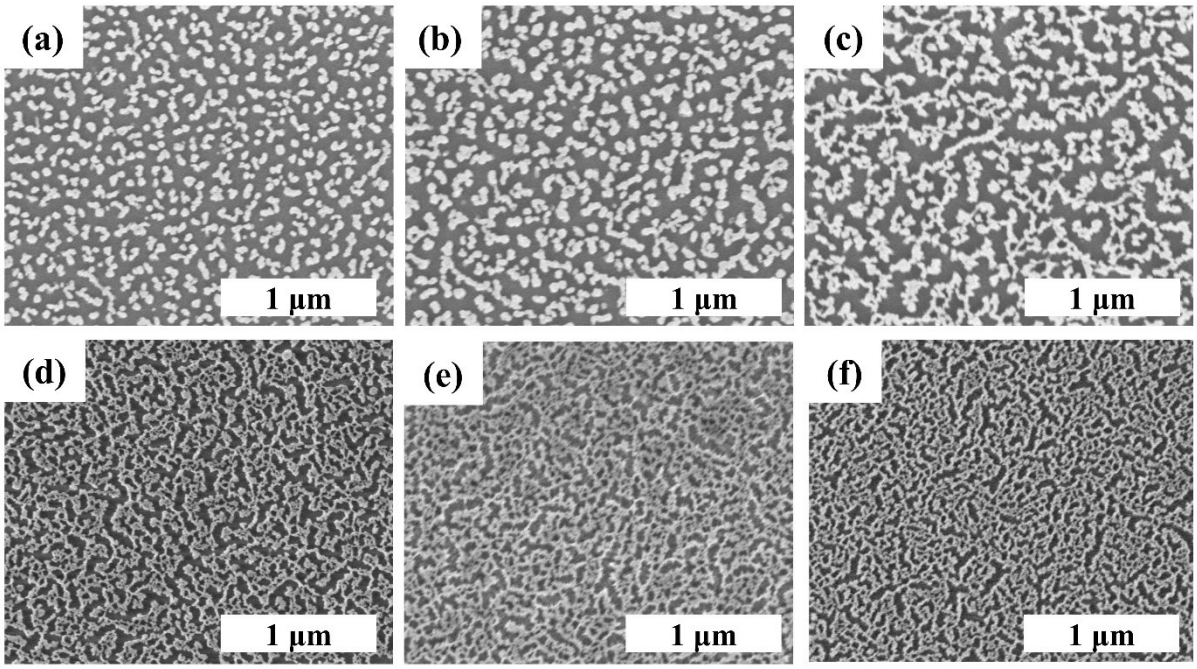

Figure S8. Top views of FESEM images of $Ni(OH)_2$ structures depending on dipping time in $K_2Ni(CN)_4$ solution with pH = 5. (a) 30 s, (b) 1 min, (c) 3 min, (d) 10 min, (e) 20 min, (f) 1 h.

Figure S8 shows the morphology of $Ni(OH)_2$ structures depending on dipping time in the $K_2Ni(CN)_4$ solution with pH =5. When the dipping time was short, the amount of the coordination was small. Thus, $Ni(OH)_2$ showed individual particles. However, as the dipping time increases, sufficient amount of the coordination occurred, resulting in the formation of porous $Ni(OH)_2$ structures. The coordination became saturated within short immersion time (10 min).

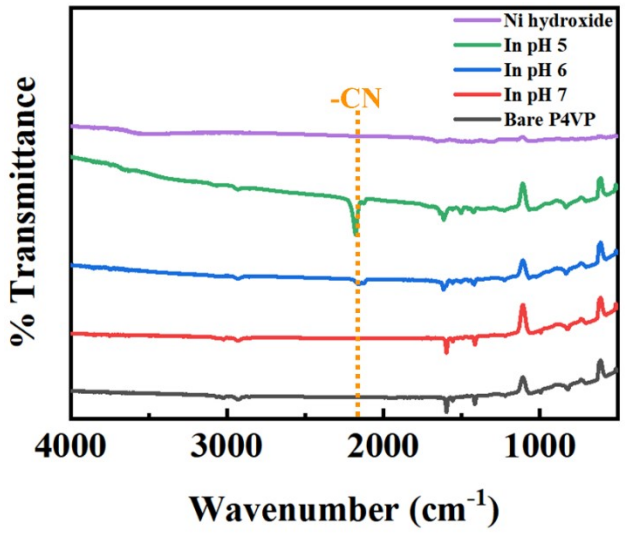

Figure S9. FTIR spectra of P4VP film before and after coordination with $K_2Ni(CN)_4$ in buffer solutions with various pH.

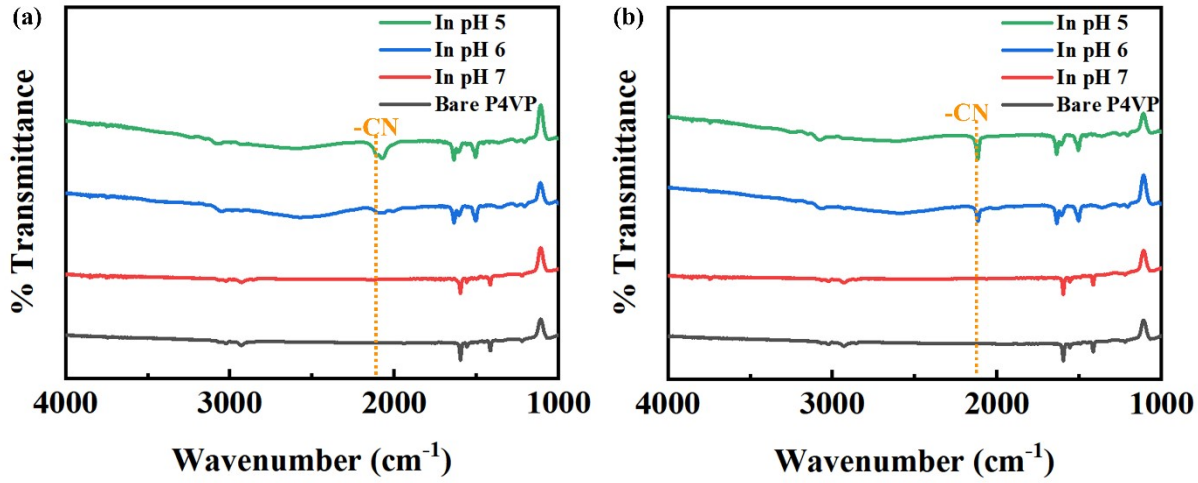

Figure S10. FTIR spectra of P4VP film before and after coordination with (a) $K_3Co(CN)_6$ (b) $K_4Fe(CN)_6$ in buffer solutions with various pH.

Figure S9 gives FTIR spectra of P4VP film before and after coordination with $K_2Ni(CN)_4$ in buffer solutions with various pHs (5~7). The intensity of the CN group (2200 ~ 2100 cm^{-1}) gradually increases with decreasing pH, implying the coordination between N+ and precursor increases with decreasing pH. Also, when complete RIE was performed, the CN peak was not observed, suggesting that all the nickel cyanide precursor was completely transformed to nickel hydroxide. Figure S10 gives FTIR spectra of P4VP film before and after coordination with $K_3Co(CN)_6$ and $K_4Fe(CN)_6$ in buffer solutions with various pH. Similar to nickel, both samples also showed increased intensity of CN group with decreasing pH.

Table S1. Comparison of specific capacitance of $Ni(OH)_2$ on various flat conductive substrates.

Material	**Shape**	**Synthetic Method**	**Max specific capacitance(F/g)**	**Electrolyte**	**Substrate(flat)**	**ref**
$Ni(OH)_2$	Porous thin film	Deposition	462 F/g at 0.0005 A/cm2	2M KOH	Stainless steel	(S1)
$Ni(OH)_2$	Porous microflower	Block copolymer template with hydrothermal	1551 F/g at 5 mV/s	6M KOH	Graphite	(S2)
$Ni(OH)_2$	Porous nanostructure	Hydrothermal	357 F/g at 5 mV/s	2M KOH	Stainless steel	(S3)
$Ni(OH)_2$	nanoplate	Hydrothermal	460 F/g at 1 A/g	6M KOH	Glassy carbon	(S4)
$Ni(OH)_2$	Porous microflower	Deposition	249 F/g at 0.05 A/g	2M KOH	Stainless steel	(S5)
$Ni(OH)_2$	Mesoporous film	Block copolymer template with solvothermal	926 F/g at 14 A/g	1M KOH	ITO	(S6)
$Ni(OH)_2$	Porous structure	Polymer-precursor coordination	780 F/g at 5 A/g 668 F/g at 10 mV/s	1M KOH	ITO	This work

References

S1 D. Dubal, V. Fulari and C. Lokhande, *Microporous Mesoporous Mater.,* 2012**, 151**, 511-516.

S2 B. P. Bastakoti, H.-S. Huang, L.-C. Chen, K. C.-W. Wu and Y. Yamauchi, *Chem. Commun.,* 2012**, 48**, 9150-9152.

S3 G. S. Gund, D. P. Dubal, S. B. Jambure, S. S. Shinde and C. D. Lokhande, *J. Mater. Chem. A,* 2013**, 1**, 4793-4803.

S4 D. Ghosh, S. Giri, A. Mandal and C. K. Das, *Chem. Phys. Lett.,* 2013**, 573**, 41-47.

S5 B. S. Singu and K. R. Yoon, *J Ind Eng Chem,* 2016**, 33**, 374-380.

S6 N. Tarutani, Y. Tokudome, M. Jobbágy, F. A. Viva, G. J. Soler-Illia and M. Takahashi, *Chem. Mater.,* 2016**, 28**, 5606-5610.